Southern Ocean control of silicon stable isotope distribution in the deep Atlantic Ocean

Gregory F. de Souza, Ben C. Reynolds, Joerg Rickli, Martin Frank, Mak A. Saito, Loes J. A. Gerringa, Bernard Bourdon

Southern Ocean control of silicon stable isotope distribution in the deep Atlantic Ocean

Gregory F. de Souza,[1] Ben C. Reynolds,[1] Jörg Rickli,[1,2] Martin Frank,[3] Mak A. Saito,[4] Loes J. A. Gerringa,[5] and Bernard Bourdon[1,6]

Received 14 June 2011; revised 4 January 2012; accepted 7 May 2012; published 19 June 2012.

[1] The fractionation of silicon (Si) stable isotopes by biological activity in the surface ocean makes the stable isotope composition of silicon (δ^{30}Si) dissolved in seawater a sensitive tracer of the oceanic biogeochemical Si cycle. We present a high-precision dataset that characterizes the δ^{30}Si distribution in the deep Atlantic Ocean from Denmark Strait to Drake Passage, documenting strong meridional and smaller, but resolvable, vertical δ^{30}Si gradients. We show that these gradients are related to the two sources of deep and bottom waters in the Atlantic Ocean: waters of North Atlantic and Nordic origin carry a high δ^{30}Si signature of $\geq$+1.7‰ into the deep Atlantic, while Antarctic Bottom Water transports Si with a low δ^{30}Si value of around +1.2‰. The deep Atlantic δ^{30}Si distribution is thus governed by the quasi-conservative mixing of Si from these two isotopically distinct sources. This disparity in Si isotope composition between the North Atlantic and Southern Ocean is in marked contrast to the homogeneity of the stable nitrogen isotope composition of deep ocean nitrate (δ^{15}N-NO_3). We infer that the meridional δ^{30}Si gradient derives from the transport of the high δ^{30}Si signature of Southern Ocean intermediate/mode waters into the North Atlantic by the upper return path of the meridional overturning circulation (MOC). The basin-scale deep Atlantic δ^{30}Si gradient thus owes its existence to the interaction of the physical circulation with biological nutrient uptake at high southern latitudes, which fractionates Si isotopes between the abyssal and intermediate/mode waters formed in the Southern Ocean.

Citation: de Souza, G. F., B. C. Reynolds, J. Rickli, M. Frank, M. A. Saito, L. J. A. Gerringa, and B. Bourdon (2012), Southern Ocean control of silicon stable isotope distribution in the deep Atlantic Ocean, *Global Biogeochem. Cycles*, *26*, GB2035, doi:10.1029/2011GB004141.

1. Introduction

[2] The oceanic biogeochemical cycle of silicon (Si) is tied to that of carbon by the important role played by diatoms – siliceous phytoplankton – in global new production [*Smetacek*, 1999; *Ragueneau et al.*, 2000, and references therein]. Diatoms additionally tend to dominate the phytoplankton community in dynamic upwelling regions [*Margalef*, 1978; *Jin et al.*, 2006] such as the Southern Ocean, which play an important role in the oceanic control of atmospheric pCO_2 [*Marinov et al.*, 2006; *Gruber et al.*, 2009]. Silicon fluxes associated with diatom productivity and export are so large that they dominantly control the oceanic Si cycle [*Tréguer et al.*, 1995]. Since diatoms preferentially incorporate the lighter isotopes of Si into their opaline frustules [*De La Rocha et al.*, 1997], diatom uptake of Si in the sunlit surface ocean alters the stable isotope composition of dissolved Si in seawater (expressed as δ^{30}Si; see section 2.2). As a result of this, seawater δ^{30}Si values trace biogeochemical processes affecting Si. Thus, constraining the mechanisms that govern the oceanic δ^{30}Si distribution allows direct inference of the pathways and processes by which Si is cycled within the ocean. This is particularly interesting in the context of an emerging paradigm of oceanic nutrient cycling [*Sarmiento et al.*, 2004, 2007; *Palter et al.*, 2010] that stresses the importance of lateral transport processes, modulated by biology in the Southern Ocean, in determining global oceanic nutrient distributions, and thus ultimately oceanic primary productivity [*Sarmiento et al.*, 2004]. In addition, a better knowledge of the processes that control the modern δ^{30}Si distribution will allow more robust interpretations of diatom opal δ^{30}Si records from deep-sea sediment cores [e.g., *De La Rocha et al.*, 1998; *Pichevin et al.*, 2009], improving our understanding of how

[1]Institute of Geochemistry and Petrology, ETH Zurich, Zurich, Switzerland.
[2]Now at Bristol Isotope Group, University of Bristol, Bristol, UK.
[3]GEOMAR, Helmholtz Centre for Ocean Research Kiel, Kiel, Germany.
[4]Woods Hole Oceanographical Institution, Woods Hole, Massachusetts, USA.
[5]Royal Netherlands Institute for Sea Research, Texel, Netherlands.
[6]Ecole Normale Supérieure de Lyon and CNRS, Lyon, France.

Corresponding author: G. F. de Souza, Institute of Geochemistry and Petrology, ETH Zurich, NW C81.1, Clausiusstrasse 25, CH-8092 Zurich, Switzerland. (desouza@erdw.ethz.ch)

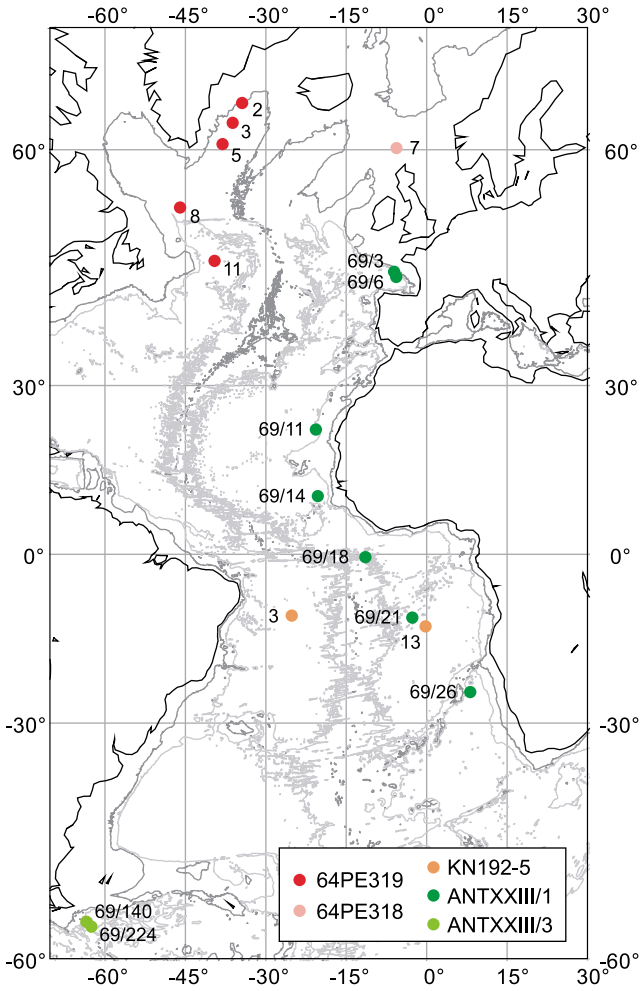

Figure 1. Map of the Atlantic Ocean illustrating locations from which samples for this study were collected. Depth contours are shown at 2000 m (dark gray) and 4000 m (light gray). Numbers represent cruise station designations. See also Table 1.

diatom productivity may have affected atmospheric pCO_2 over glacial–interglacial cycles [*Brzezinski et al.*, 2002; *Matsumoto et al.*, 2002; *Crosta et al.*, 2007]. Together, these two complementary issues provide strong motivation to study the modern oceanic δ^{30}Si distribution, particularly in the Atlantic Ocean.

[3] The Atlantic is the best studied of the major ocean basins. Both its physical and chemical oceanography have been the subject of intense study, such that much is known about Atlantic circulation [e.g., *Wüst*, 1935; *Reid*, 1989; *Schmitz and McCartney*, 1993; *Dickson and Brown*, 1994; *Schmitz*, 1996; *Stramma and England*, 1999; *Lumpkin and Speer*, 2003] as well as the distribution of biogeochemical tracers [e.g., *Broecker et al.*, 1976; *Kawase and Sarmiento*, 1985; *Broecker et al.*, 1991; *Tsuchiya et al.*, 1994; *Sarmiento et al.*, 2007]. This well-founded understanding of the system, combined with the fact that the deep Atlantic exhibits strong meridional contrasts in physical and chemical tracers, makes the Atlantic Ocean ideally suited to constraining processes determining the behavior of a relatively novel isotopic tracer such as seawater δ^{30}Si.

[4] In-depth studies of seawater δ^{30}Si [*Varela et al.*, 2004; *Cardinal et al.*, 2005; *Reynolds et al.*, 2006a; *Beucher et al.*, 2008; *Fripiat et al.*, 2011] have thus far focused on high-nutrient, low-chlorophyll regions that are the key areas for ocean–climate interaction and overlie opal-rich sediments. The Atlantic Ocean has been somewhat neglected, most likely due to its modest contribution to biological Si cycling in the modern ocean, reflected by a very low opal export flux for its area (5% of global export) [*Sarmiento et al.*, 2007]. However, the fact that the primary formation regions of the deep and bottom waters that fill the global ocean are situated at its northern and southern end [*Warren*, 1981] makes the Atlantic highly relevant to the global oceanic Si cycle. Furthermore, as it contains the world's youngest and least Si-rich deepwaters (0–300 yr ventilation ages) [*Matsumoto*, 2007], a firm handle on the δ^{30}Si distribution in the deep Atlantic is crucial to better resolve an interesting feature of the oceanic δ^{30}Si distribution: it appears that the North Atlantic and North Pacific have distinct deepwater δ^{30}Si values, which would contrast the homogeneity of the stable nitrogen isotopic composition of deep oceanic nitrate, δ^{15}N-NO_3 [e.g., *Sigman et al.*, 2009]. However, the Atlantic end of this interbasin gradient is represented by only three depth profiles near Bermuda [*De La Rocha et al.*, 2000]. This poor spatial resolution hinders a robust analysis of the mechanisms leading to the observed distribution, and modeling studies have delivered conflicting results in this regard [*Wischmeyer et al.*, 2003; *Reynolds*, 2009].

[5] In order to characterize the δ^{30}Si systematics of the Atlantic Ocean, we have analyzed a suite of Atlantic seawater samples from Denmark Strait to Drake Passage. A companion paper (G. F. de Souza et al., Strong physical control on silicon stable isotope distribution in the Atlantic thermocline, manuscript in preparation, 2012) discusses the δ^{30}Si distribution in the main thermocline, while this paper focuses on the Atlantic δ^{30}Si distribution below 2000 m water depth. We show that the deep Atlantic exhibits a strong meridional δ^{30}Si gradient, which we relate to the interaction of the global meridional overturning circulation (MOC) with biological Si cycling processes at high southern latitudes, thereby providing evidence for the importance of a Southern Ocean source of nutrients to the low-latitude thermocline. Furthermore, we show that the distribution of seawater δ^{30}Si values robustly confirms earlier interpretations of quasi-conservative behavior of Si at depth in the Atlantic Ocean [*Broecker et al.*, 1991].

2. Methods

2.1. Sample Collection

[6] A total of 84 seawater samples are included in this study (Figure 1 and Table 1). These include 25 samples originally collected for analysis of neodymium and hafnium isotopic composition [*Rickli et al.*, 2009] at 7 stations in the eastern Atlantic Ocean during expedition ANT XXIII/1 of R/V *Polarstern* (October–November 2005). Two detailed depth profiles (17 samples each) from the tropical Brazil and Angola Basins were collected during expedition KN192-5 of R/V *Knorr* (November–December 2007). A further 23 samples were collected at 6 stations along GEOTRACES section GA02 in the North Atlantic, during

Table 1. Location of Expeditions and Stations From Which Samples Were Collected for This Study[a]

Cruise	Region	Station	Location	Latitude	Longitude	Water Depth (m)
64PE318	North Atlantic	7	Faroe–Shetland Channel	60° 6′ N	5° 48′ W	1060
64PE319	North Atlantic	2	Irminger Basin	64° N	34° 15′ W	2224
		3	Irminger Basin	62° 21′ N	36° W	2710
		5	Irminger Basin	60° 26′ N	37° 55′ W	2944
		8	Labrador Sea	54° 4′ N	45° 50′ W	3444
		11	Newfoundland Basin	47° 48′ N	39° 24′ W	4566
ANT XXIII/1	Eastern Atlantic (subtropical and tropical)	PS 69/3	Bay of Biscay	46° 25′ N	5° 55′ W	4360
		PS 69/6	Bay of Biscay	45° 45′ N	5° 32′ W	4620
		PS 69/11	Canary/Cape Verde Basin	22° 30′ N	20° 30′ W	4136
		PS 69/14	Cape Verde Basin	10° 37′ N	20° 8′ W	4924
		PS 69/18	Guinea Basin/Chain Fracture Zone	0° 42′ S	11° 16′ W	3879
		PS 69/21	Angola Basin	11° 52′ S	2° 31′ W	5747
		PS 69/26	Cape Basin	25° S	8° 17′ E	4778
KN 192–5	Tropical Atlantic (eastern and western)	3	Brazil Basin	11° 30′ S	25° W	4400
		13	Angola Basin	13° 29′ S	0° W	5400
ANT XXIII/3	South Atlantic	PS 69/140	Drake Passage	56° 26′ S	63° 18′ W	3984
		PS 69/224	Drake Passage	56° 56′ S	62° 21′ W	4096

[a]See also Figure 1.

expeditions 64PE318 and 64PE319 of R/V *Pelagia* (April–May 2010). In addition, two samples from Drake Passage (R/V *Polarstern* expedition ANT XXIII/3) were procured. All samples were filtered onboard using 0.45 μM nitrocellulose (*Polarstern*), 0.45 μM polycarbonate (*Knorr*) or 0.2 μM cellulose acetate (*Pelagia*) filters. Samples from *Polarstern* expeditions were acidified onboard with 0.1% v/v distilled 9.5 M HCl [*Rickli et al.*, 2009], while samples from expeditions KN192-5, 64PE318 and 64PE319 were acidified with 0.1% v/v distilled 6 M HCl in the laboratory at least 12 hr before preconcentration of Si.

2.2. Sample Preconcentration and Analysis

[7] We typically process 64 nmoles (1.8 μg) of Si for each mass-spectrometric analysis of Si stable isotope composition. Prior to the chromatographic separation of Si from sea salt, Si is preconcentrated by coprecipitation with brucite using a method modified from *Karl and Tien* [1992]. This preconcentration decreases the associated salt cation and anion matrix by more than two orders of magnitude, permitting the use of small ion exchange columns. Our two-step precipitation procedure (similar to that used by *Reynolds et al.* [2006a]) achieves Si yields generally in excess of 99% (and always >97.5%): in a first step, ∼10% of seawater Mg is precipitated as $Mg(OH)_2$ by adding ∼1% v/v of 1 M NaOH solution (semiconductor grade; Sigma-Aldrich) to the pH-neutralized seawater sample. This solution is shaken for 1 hr and allowed to react and settle for 24 hr before being centrifuged. The second precipitation step is carried out by further addition of 1 M NaOH to precipitate ∼10% of the remaining sample Mg, followed by shaking for 1 hr, settling for at least 24 hr and centrifuging. The supernatant is removed and the yield of the coprecipitation determined by photospectrometric analysis of supernatant Si concentration using the molybdate blue method [*Strickland and Parsons*, 1968]. The precipitate is then dissolved in a small volume of 6 M HCl and diluted with ultrapure water (>18.2 MΩcm) to 64 μM (1.8 ppm) Si, at which point it contains ≤53 mM Mg (i.e. ≤0.11 meq Mg/ml) as its main cationic matrix at a pH of 2–3. One milliliter of this solution is passed through a cation-exchange column with a retention capacity of 1.7 meq (1 mL AG50W-X8; BioRad Laboratories) to separate uncharged H_4SiO_4 from the cationic matrix. The uncharged and anionic matrix, which consists primarily of Cl^-, SO_4^{2-} and PO_4^{3-}, is not removed by this method, such that the final solution contains ∼1.5 mM Cl^- (mainly from HCl), ∼1 μM seawater SO_4^{2-}, and a PO_4^{3-} concentration that depends on the seawater P:Si ratio (which ranges from ∼0.02–0.2). Anion doping tests have shown that the presence of these anions does not result in analytical artifacts; in fact, the insensitivity of our analytical setup to the presence of SO_4^{2-} has been previously documented by *Georg et al.* [2006], a finding that contrasts with the matrix effects observed by *van den Boorn et al.* [2009] using a different analytical system, perhaps due to the different sample introduction systems used. We verified the accuracy of our seawater δ^{30}Si analyses using the standard addition method applied to isotopic analyses by *Tipper et al.* [2008] (see section A in Text S1 in the auxiliary material).[1]

[8] The purified Si solution is analyzed for Si stable isotope composition using a high-resolution multicollector inductively coupled plasma mass spectrometer (*NuPlasma* 1700; Nu Instruments, UK) in static mode by standard–sample bracketing, with one δ^{30}Si analysis consisting of 5 bracketed measurements (36 × 5 s integrations each) of the sample. Detailed descriptions of the chromatographic separation and mass-spectrometric methods used are given by *Georg et al.* [2006].

[9] Silicon stable isotope composition is reported as the permil deviation from the standard reference material NBS28, δ^{30}Si, which is defined as:

$$\delta^{30}\mathrm{Si} = \left(\frac{\left(\frac{^{30}\mathrm{Si}}{^{28}\mathrm{Si}}\right)_{\mathrm{sample}}}{\left(\frac{^{30}\mathrm{Si}}{^{28}\mathrm{Si}}\right)_{\mathrm{NBS\ 28}}} - 1 \right) \times 1000\ [‰]$$

[1]Auxiliary materials are available in the HTML. doi:10.1029/2011GB004141.

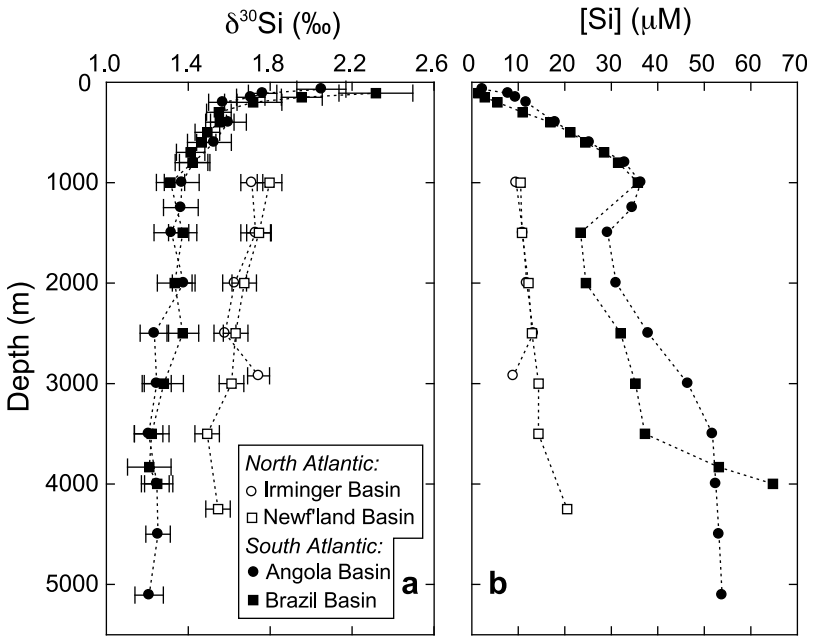

Figure 2. Depth profiles of (a) δ^{30}Si values and (b) Si concentrations. The western North Atlantic (Irminger and Newfoundland Basins; 64PE319 Stas 5 and 11) is offset toward higher δ^{30}Si values and lower [Si] than the South Atlantic (Brazil and Angola Basins; KN192-5 Stas 3 and 13). Note the increase in δ^{30}Si at the base of the water column in the Irminger Basin, associated with the lower [Si] of Denmark Strait Overflow Water. See auxiliary material for δ^{30}Si and [Si] depth profiles from all stations included in this study. Error bars on δ^{30}Si values are $2\sigma_{SEM}$ in this and all following figures, except where mentioned otherwise.

The long-term external reproducibility of our δ^{30}Si analyses is ±0.12‰ ($2\sigma_{SD}$), as estimated from the variance of ~300 analyses of the secondary isotopic standard Diatomite [*Brzezinski et al.*, 2006] over >3 yr. The average δ^{30}Si value of Diatomite measured over this period is +1.22 ± 0.01‰ ($2\sigma_{SEM}$), consistent with the inter-laboratory comparison study of *Reynolds et al.* [2007]. Except in the case of near-surface samples with low amounts of Si, reported sample δ^{30}Si values are the mean of at least 3, and up to 11, complete replicate analyses in at least 2 separate analytical sessions. External errors on the seawater data, reported as 2 standard errors of the mean ($2\sigma_{SEM}$), are usually ±0.07‰ or better (see Table S1 in the auxiliary material). Error bars shown in all figures are external $2\sigma_{SEM}$. In the following, the notations Si, [Si] and δ^{30}Si will refer to *dissolved* silicon (i.e. silicic acid), its concentration, and its stable isotope composition respectively.

3. Results

[10] Depth profiles of δ^{30}Si (see examples in Figure 2a) show the typical increase in δ^{30}Si values toward the surface that is expected from the preferential uptake of lighter Si isotopes by diatoms in the surface ocean. Values of δ^{30}Si range from approximately +1.2‰ in bottom waters to almost +3‰ in the surface mixed layer (Table S1 in the auxiliary material; all depth profiles are illustrated in Figures S1–S4 in Text S1 of the auxiliary material). The gradient toward higher δ^{30}Si values is largest in the upper ocean, above the salinity minimum at ~1000 m associated with Antarctic Intermediate Water (AAIW) in the South Atlantic. Below this, δ^{30}Si gradients are much smaller, but δ^{30}Si values generally continue to decrease with depth, with the exception of the northernmost North Atlantic (Irminger Basin; 64PE319 Stas 3 and 5), where δ^{30}Si values increase slightly with depth near the very bottom of the water column (Figure 2b), associated with stronger gradients in temperature and [Si] (Table S1 in the auxiliary material). Furthermore, the entire water column exhibits a clear difference in δ^{30}Si values between the North and South Atlantic (Figure 2). At temperate northern latitudes around 45°N, the western Atlantic (64PE319 Sta 11) exhibits lower [Si] and higher δ^{30}Si values than the eastern Atlantic (ANTXXIII/1 Stas 3 and 6; Figure S2).

[11] A remarkably strong coherence in the δ^{30}Si systematics of the entire sampled Atlantic is illustrated by the relationship between concentration and isotopic composition of Si. Graphs of δ^{30}Si values versus the reciprocal of silicon concentration, 1/[Si] (Figure 3), reveal that samples from all regions exhibit the same relationship between these parameters, even when their δ^{30}Si depth profiles exhibit clear differences (Figure 2). In Figure 3a, the existence of two line ararrays with different slopes is apparent. These arrays intersect at a δ^{30}Si value of +1.55–1.6‰ and 1/[Si] of 0.09–0.06, corresponding to a potential density σ_θ of 26.75–27.00 (water depth 300–400 m), i.e. in the range of densities of Subantarctic Mode Water (SAMW) in the Atlantic [*Larqué et al.*, 1997; *Sallée et al.*, 2010].

[12] In the following discussion, we describe and discuss the deep Atlantic δ^{30}Si distribution below 2000 m water depth (section 4.1), and draw upon the δ^{30}Si signature of the

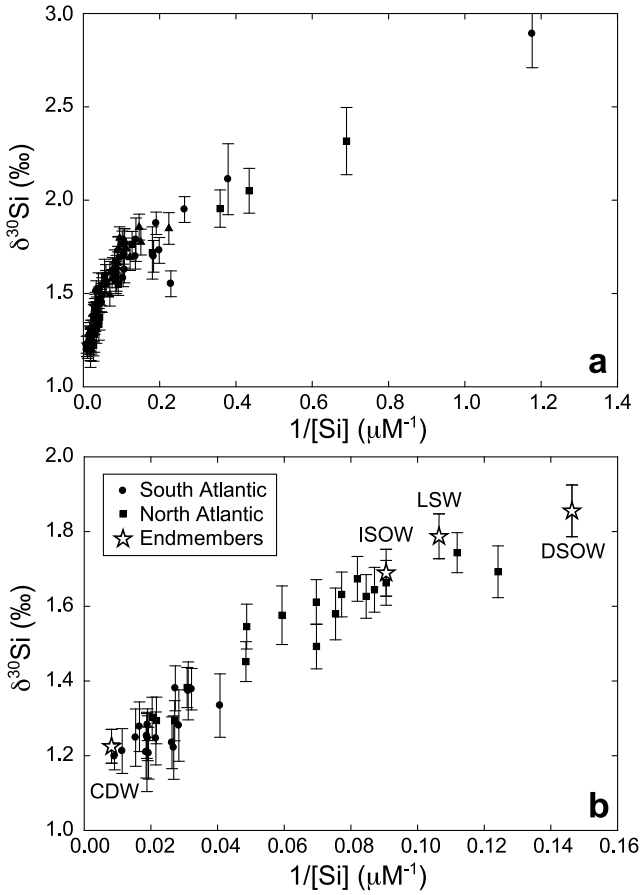

Figure 3. Silicon isotope systematics of the Atlantic Ocean, plotted as mixing diagrams of δ^{30}Si vs.1/[Si]. (a) All samples and (b) the water column below ~2000 m. A clear and coherent relationship between δ^{30}Si and 1/[Si] is seen. The mixing diagram in Figure 3a exhibits two linear relationships between δ^{30}Si and 1/[Si], intersecting at δ^{30}Si values of +1.55–1.6‰. Figure 3b focuses on the Si isotope systematics of the deep Atlantic below ~2000 m, emphasizing the tightness of the linear relationship at depth. Stars in Figure 3b represent the deep water mass end-members of Southern Ocean and North Atlantic origin (CDW: Circumpolar Deep Water, ISOW: Iceland-Scotland Overflow Water, LSW: Labrador Seawater, DSOW: Denmark Strait Overflow Water). Note that the water mass labeled as ISOW for clarity would more correctly be named Faroe-Shetland Overflow Water, which is a dominant component of ISOW [*Dickson and Brown*, 1994].

intermediate and upper Atlantic to explain its ultimate origin in the context of the MOC (sections 4.2–4.4).

4. Discussion

4.1. Quasi-Conservativity of Si

[13] It is a striking feature of the deep Atlantic δ^{30}Si distribution that the North Atlantic water column exhibits consistently higher δ^{30}Si values than the South Atlantic (Figure 2 and Table S1 in the auxiliary material). In a plot of δ^{30}Si values against the reciprocal of Si concentration, 1/[Si], this meridional gradient is expressed as a linear array for water samples below ~2000 m (Figure 3b). The existence of such a linear relationship is indicative of conservative mixing between two distinct reservoirs, or end-members (see, e.g., *Albarède* [1996] for a derivation). The deep Atlantic δ^{30}Si systematics thus strongly suggests that the distribution of Si in the deep Atlantic is controlled by binary mixing, with no significant sources or sinks. This would imply that Si is quasi-conservative in the deep Atlantic, which might intuitively seem unlikely for a biologically cycled nutrient. As we show below, however, it can be demonstrated that this is indeed the case in the deep Atlantic Ocean.

[14] *Broecker et al.* [1991], and more recently *Sarmiento et al.* [2007], have shown that while the effect of opal dissolution on deep Atlantic [Si] can be resolved by careful analysis, this effect is of minor importance (<5% contribution) in controlling deep [Si]. Similarly, *Anderson and Sarmiento* [1994] find that "the remineralization signal in the deep Atlantic is practically non-existent". In the case of Si, this is partially due to the low Atlantic opal productivity [*Sarmiento et al.*, 2007], but the leading-order control is the order-of-magnitude disparity in [Si] between the two water masses filling the deep Atlantic, i.e. North Atlantic Deep Water (NADW, [Si] < 20 μM) and Antarctic Bottom Water (AABW, [Si] ~ 120 μM). This pronounced [Si] contrast means that admixture of Si-rich AABW to Si-poor NADW produces large [Si] changes, such that mixing of these two water masses exerts by far the strongest control on variations in Atlantic [Si] below a water depth of ~2000 m. Silicon concentrations are thus closely correlated with conservative and quasi-conservative tracers of water mass mixing such as salinity [*Holfort and Siedler*, 2001] and PO_4^* [*Broecker et al.*, 1991] (see also section B in Text S1 in the auxiliary material) in the deep Atlantic, with the exception of a few local anomalies [e.g., *van Bennekom and Berger*, 1984].

[15] The influence of the contrasting northern and southern water masses on the deep Atlantic δ^{30}Si systematics is apparent in Figure 3b. Low δ^{30}Si values are associated with the high Si concentrations of AABW, while the highest δ^{30}Si values are observed for the precursors of NADW, i.e. the dense Si-poor overflows from the Nordic seas (Denmark Strait Overflow Water and Iceland-Scotland Overflow Water, DSOW and ISOW) as well as Labrador Seawater (LSW) [*Dickson and Brown*, 1994]. These northern and southern deepwater sources thus represent the two isotopic end-members inferred above to be controlling the Atlantic δ^{30}Si distribution. By calculating the deviation of measured δ^{30}Si values from those expected from pure mixing of these end-members, we can quantify the degree of conservativity of Si. Following *Gruber* [1998], we utilize the quasi-conservative tracer PO_4^* [*Broecker et al.*, 1991] to independently calculate the contribution of North Atlantic waters f_{NA} to each sample (see section B in Text S1 in the auxiliary material). The δ^{30}Si value expected from pure binary mixing, $\delta^{30}Si_{mix}$, is then:

$$\delta^{30}\mathrm{Si}_{mix} = \frac{f_{NA}\delta^{30}\mathrm{Si}_{NA}[\mathrm{Si}]_{NA} + (1-f_{NA})\delta^{30}\mathrm{Si}_{SO}[\mathrm{Si}]_{SO}}{f_{NA}[\mathrm{Si}]_{NA} + (1-f_{NA})[\mathrm{Si}]_{SO}}$$

where *NA* and *SO* refer to the North Atlantic and Southern Ocean components respectively, and $\delta^{30}Si_i$ and $[Si]_i$ are the isotopic composition and concentration of Si in the

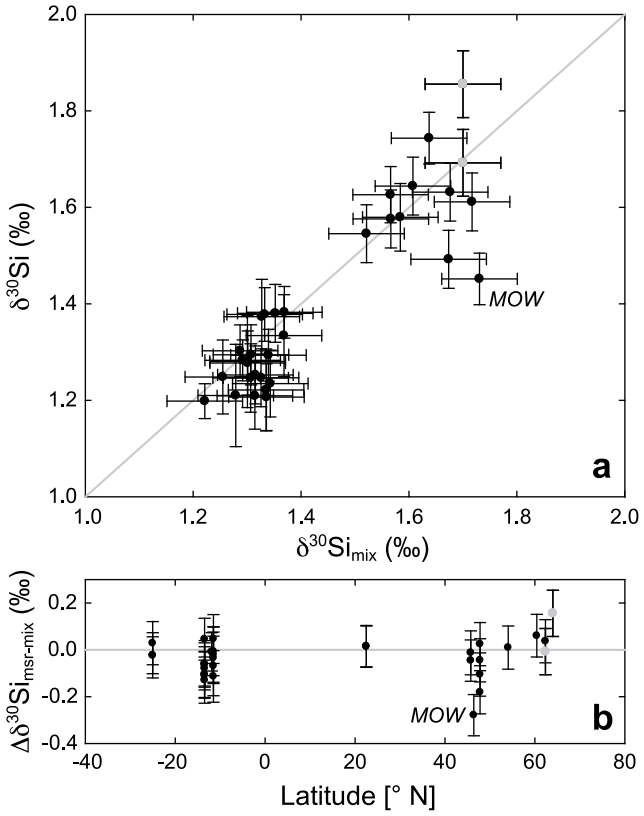

Figure 4. Quantifying the degree of conservativity of δ^{30}Si for samples below ~2000 m. (a) A cross-plot of measured δ^{30}Si values with $\delta^{30}Si_{mix}$ values based on end-member contribution calculations (see section B in Text S1 in the auxiliary material) shows good correspondence between the two values. Note that the sample affected by Mediterranean Outflow Water (MOW) lies most strongly away from the 1:1 line. (b) The latitudinal distribution of the deviation of measured δ^{30}Si values from those expected from mixing ($\Delta\delta^{30}Si_{msr-mix}$; see text) for the same samples, emphasizing that binary mixing explains deep δ^{30}Si values over the entire latitudinal range, with most sample plotting within error of $\Delta\delta^{30}Si_{msr-mix} = 0$. Errors are propagated from δ^{30}Si and $\delta^{30}Si_{mix}$ values. Samples whose PO_4^* values were corrected to the North Atlantic end-member value of 0.76 μmol/kg (see section B in Text S1 in the auxiliary material) are indicated as gray datapoints in both panels.

component *i*. The deviation of the measured value from this value is given by $\Delta\delta^{30}Si_{msr-mix}$, defined as:

$$\Delta\delta^{30}Si_{msr-mix} = \delta^{30}Si_{measured} - \delta^{30}Si_{mix}$$

Values of $\Delta\delta^{30}Si_{msr-mix}$ for the deep Atlantic are, with some notable exceptions, generally smaller than the associated uncertainties (Figure 4b and section B in Text S1 in the auxiliary material). This close correspondence of measured and calculated δ^{30}Si values demonstrates that Si is predominantly quasi-conservative in the deep Atlantic. The sample most strongly offset from the 1:1 line in Figure 4a is a sample from the Bay of Biscay, whose chemistry (PO_4^*, δ^{30}Si, or both) is influenced by Mediterranean Overflow Water [*Gruber*, 1998]. There is a slight tendency of measured δ^{30}Si values in the South Atlantic to be marginally lower than calculated values (Figure 4). These offsets are associated with samples from the deep Angola basin, where seawater neodymium isotope compositions appear to be affected by the Congo Fan [*Rickli et al.*, 2009]. The observed slight δ^{30}Si deviations from pure mixing might thus indicate that Si release from the Congo Fan [*van Bennekom and Berger*, 1984; *Ragueneau et al.*, 2009] plays a minor role in modulating deep δ^{30}Si values here.

[16] The strongest control on the deep Atlantic δ^{30}Si distribution, however, is the physical circulation: Antarctic Bottom Water advects a low δ^{30}Si value of around +1.2‰ into the Atlantic from the south, while high δ^{30}Si values of +1.7‰ to +1.85‰ are introduced into the North Atlantic by the NADW-precursors. Mixing between these water masses results in the observed small δ^{30}Si gradients with depth at individual stations, but also in the large-scale meridional δ^{30}Si gradient. The propagation of the high δ^{30}Si signal from the North Atlantic also traces the path of deepwater circulation: the midlatitude western Atlantic water column, which is strongly influenced by the deep western boundary current transporting NADW southwards, displays both lower [Si] and higher δ^{30}Si values than the eastern Atlantic at the same latitude (Figure S2 and Table S1).

[17] By documenting the quasi-conservativity of Si and emphasizing the dominant influence of circulation on the δ^{30}Si distribution, our data robustly confirm minimal influence of opal dissolution on the Si distribution in the Atlantic [*Broecker et al.*, 1991; *Sarmiento et al.*, 2007], and indicate that processes such as boundary exchange, which has been suggested to result in a significant flux of Si into the global ocean [*Jeandel et al.*, 2009], are insignificant in determining the distribution of Si in the deep Atlantic.

4.2. Origin of δ^{30}Si Signatures

[18] The distinct δ^{30}Si signatures of North Atlantic and Southern Ocean waters are at odds with their homogeneity in δ^{15}N-NO_3 [e.g., *Sigman et al.*, 2009]. Such a difference between these two broadly comparable nutrient isotope systems is surprising, and must reflect a dissimilarity in the oceanic cycles of Si and N. In the following, we first elucidate how the North Atlantic and Southern Ocean water masses obtain their distinct δ^{30}Si signatures, and the implications that this has for the oceanic Si cycle. Comparison with the δ^{15}N-NO_3 system then allows us to suggest likely causes of the difference between oceanic δ^{30}Si and δ^{15}N-NO_3 distributions.

[19] *Toggweiler et al.* [2006] introduced a cartoon representation of the ocean circulation that provides an illustrative schematic framework for the following arguments. They separate the MOC into two domains, or "loops", as shown in Figure 5: a southern loop dominated by AABW, and a northern loop dominated by NADW, fed by northward flow through the thermocline. These two domains interact to form Circumpolar Deep Water (CDW) that upwells in the Southern Ocean, feeding both circulation loops. The prolonged exposure of the northern loop to biological activity at the surface leads to a strong depletion in nutrients. Below, we explain the origin of deepwater δ^{30}Si values in the context of this schematic, beginning with the southern loop.

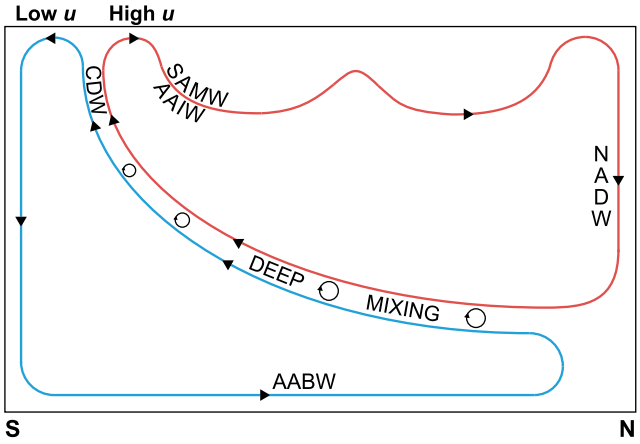

Figure 5. A cartoon illustration of large-scale features of the meridional overturning circulation, modified from *Toggweiler et al.* [2006]. u = nutrient utilization.

[20] Antarctic Bottom Water forms in the high latitudes of the Southern Ocean, primarily in the Weddell Sea [*Orsi et al.*, 1999], through a series of interactions of surface waters with shelf waters densified by brine rejection [*Foster and Carmack*, 1976; *Huhn et al.*, 2008]. Due to a combination of high upwelling rates and micronutrient- and light-limitation of plankton growth [e.g., *Chisholm and Morel*, 1991], these waters all contain high levels of macronutrients. The waters brought to the surface Antarctic by upwelling of CDW thus experience little Si depletion before they sink and are incorporated into AABW (Figure 5), such that their nutrient properties remain similar to those of CDW. Furthermore, the sinking waters entrain significant volumes of surrounding water as they traverse the slope, and experience strong mixing in the region of the Antarctic Circumpolar Current, such that they exit the Southern Ocean containing a considerable admixture of CDW [e.g., *Mantyla and Reid*, 1983]. Considering this formation process, it is unsurprising that the δ^{30}Si value of AABW is indistinguishable from that of CDW at about +1.2‰ [*Cardinal et al.*, 2005; this study], a value that in turn must reflect the balance of silicon inputs to and outputs from the Southern Ocean.

[21] The North Atlantic water masses that contribute to NADW (i.e. DSOW, ISOW and LSW), on the other hand, are formed by the buoyancy loss of surface waters from lower latitudes that are transported into the high-latitude North Atlantic by the Gulf Stream/North Atlantic Current [e.g., *Hansen and Østerhus*, 2000; *McCartney and Mauritzen*, 2001; *Brambilla et al.*, 2008], as represented by the northern loop of Figure 5. Deep convection in the subpolar North Atlantic leads to the formation of Subpolar Mode Water, including its densest type, Labrador Seawater [*McCartney and Talley*, 1982; *Brambilla et al.*, 2008]. Similarly, the Nordic overflows DSOW and ISOW are fed by light-to-dense conversions of waters of shallow North Atlantic origin in the Norwegian Sea [*Mauritzen*, 1996; *Hansen and Østerhus*, 2000; *Eldevik et al.*, 2009]. In both of these cases, the surface waters that experience buoyancy loss have very low [Si] [*Garcia et al.*, 2010], such that, although they may have elevated δ^{30}Si values as a result of biological uptake of Si, they have limited potential to influence the δ^{30}Si value of a water mass formed by deep convection. This is because the Si budget – and thus δ^{30}Si signature – of the homogenized water mass formed by convection is strongly weighted (~95%) toward the entrained subsurface waters. In the case of both LSW and the Nordic overflows, these subsurface waters possess North Atlantic characteristics [*McCartney and Talley*, 1982; *McCartney and Mauritzen*, 2001]. Thus, in order to trace the origin of the high δ^{30}Si value of NADW, we must understand what controls the Si budget, and thus δ^{30}Si value, of the North Atlantic subsurface.

4.3. Influence of the Large-Scale Circulation

[22] The northern loop of Figure 5 indicates that the deep export of NADW from the North Atlantic is compensated by northward flow of waters in the upper ocean. This feature is supported by numerous observational constraints and inverse models [*Schmitz and McCartney*, 1993; *Schmitz*, 1995, 1996; *Ganachaud and Wunsch*, 2000; *Sloyan and Rintoul*, 2001; *Lumpkin and Speer*, 2003, 2007]. The flow of upper Atlantic waters into the North Atlantic is associated with a northward transport of nutrients in the subsurface [e.g., *Rintoul and Wunsch*, 1991] that strongly influences the North Atlantic nutrient budget; indeed, the advective nutrient transport associated with the MOC is vital in maintaining North Atlantic nutrient stocks in the long term [*Williams et al.*, 2006; *Palter and Lozier*, 2008]. Such a dominant term in the nutrient mass balance should be a strong control on the δ^{30}Si value of the North Atlantic subsurface. Below, we estimate a δ^{30}Si value for this input.

[23] Since the magnitude of diapycnal mixing in the main thermocline is small [*Ledwell et al.*, 1993; *Toggweiler and Samuels*, 1993; *Toole et al.*, 1994; *Schmittner et al.*, 2009], it is likely that the nutrients transported by the northward flow in the Atlantic thermocline are dominantly sourced from the waters that introduce nutrients into the thermocline in the south, i.e. SAMW and AAIW [*Tsuchiya*, 1989; *Schmitz and McCartney*, 1993; *Sarmiento et al.*, 2004; *Williams et al.*, 2006; *Palter and Lozier*, 2008; *Palter et al.*, 2010]. The importance of a southern source of nutrients to the thermocline is also indicated by the δ^{30}Si systematics: the intersect between the upper- and deeper-ocean δ^{30}Si–1/[Si] relationships occurs at potential densities corresponding to these water masses. The intermediate cross-equatorial transport into the North Atlantic takes place in the σ_θ interval 26.8–27.2 [*Schmitz*, 1995, and references therein], which closely corresponds to the density range of SAMW and AAIW in the South Atlantic (σ_θ = 26.8–27.3 [*Larqué et al.*, 1997; *Sallée et al.*, 2010]). The corresponding samples in our South Atlantic dataset have δ^{30}Si values ranging from +1.45‰ to +1.6‰, with an average of +1.5‰ when weighted by [Si] in the water mass. The NADW complex being transported southwards at 45°N has a concentration-weighted average only slightly higher than this (+1.6‰). In the context of the large-scale circulation represented by Figure 5, this similarity suggests that the 0.4‰ offset in δ^{30}Si values between NADW and AABW is largely the result of the δ^{30}Si difference between the water masses of Southern Ocean origin, i.e. between AABW and SAMW/AAIW.

[24] We test this hypothesis by performing a sensitivity test in a simple box model of the ocean, as shown in Figure 6a. This 8-box model is a modification of the 7-box

model of *Reynolds* [2009] (based on *Toggweiler* [1999]), altered to more clearly separate the two high-latitude end-members that are our focus of interest here. As illustrated in Figure 6a, the circulation simulated by this model bears a close resemblance to the schematic view of *Toggweiler et al.* [2006] (Figure 5). The model produces a [Si] gradient between the Si-rich deepwaters of the "Southern" Ocean (box *ds*) and the Si-poor North Atlantic deepwaters (box *dn*; Figure 6b). Although it overestimates [Si] in the surface Southern Ocean (boxes *p* and *s*), the model successfully captures the latitudinal gradients in surface [Si] and δ^{30}Si values that are a key feature of the Southern Ocean Si distribution [*Varela et al.*, 2004; *Sarmiento et al.*, 2004; *Fripiat et al.*, 2011]. The model also produces a large-scale δ^{30}Si gradient between North Atlantic and Southern Ocean deepwaters (Figure 6b). Sensitivity analyses by *Reynolds* [2009] have shown that this deepwater δ^{30}Si gradient is a robust model feature whose presence is not dependent on the choice of parameter values (see also section D in Text S1 in the auxiliary material). In order to identify the ultimate source of this gradient, we perform a simple sensitivity test: by "switching off" isotope fractionation during utilization in the surface Southern Ocean, the model is prevented from creating an isotopic difference between intermediate and deep Southern Ocean waters. This approach has the advantage of leaving the elemental distribution of Si unaffected, which considerably simplifies the interpretation of model results. In this test configuration (Figure 6c), the δ^{30}Si value of the North Atlantic is essentially identical to that of the deep Southern Ocean, despite isotope fractionation in the low- and high northern latitude surface ocean and a deep [Si]-gradient identical to that of the standard configuration. The presence of a deep δ^{30}Si gradient in the model is thus dependent upon the introduction of a high-δ^{30}Si signal into intermediate waters from the surface Southern Ocean. This model result thus supports the inference that the transport of Si with a high δ^{30}Si value into the North Atlantic by the upper return path of the MOC must play an important role in producing the δ^{30}Si difference between NADW and AABW. Silicon uptake and isotope fractionation by diatoms in the surface Southern Ocean thus effectively fractionate Si isotopes between the two MOC loops of Figure 5.

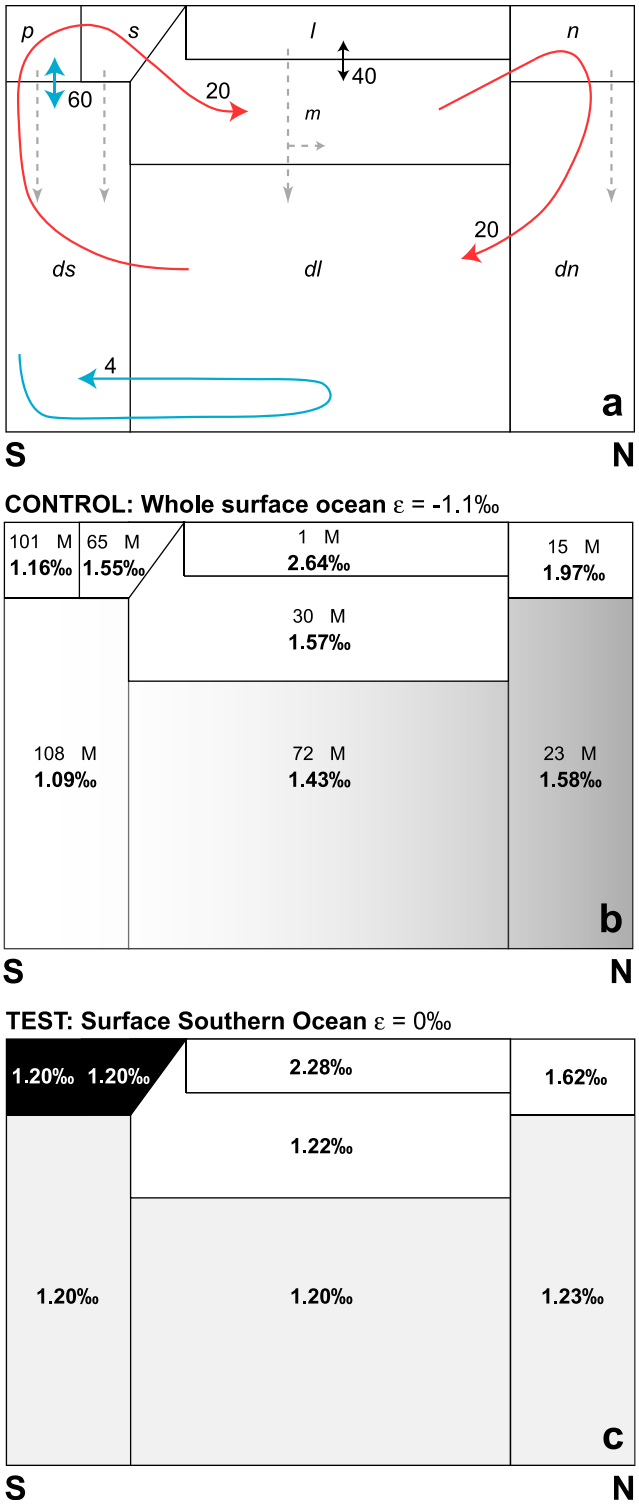

4.4. Si and N Cycles

[25] If the contrast in the δ^{30}Si signatures of NADW and AABW is due in large part to a δ^{30}Si difference between shallow and deep Southern Ocean waters, we should address (a) what in turn causes this difference, and (b) why this process does not result in a similar contrast in δ^{15}N-NO_3. A comparison of Southern Ocean δ^{30}Si and δ^{15}N–NO_3 data is highly instructive in this regard (Figures 7 and 8) [*Sigman et al.*, 2000; *Cardinal et al.*, 2005; *DiFiore et al.*, 2006].

Figure 6. Results of the 8-box model. (a) The model architecture, modified from *Toggweiler* [1999], with water fluxes in Sv (solid lines) and particulate export (dashed gray arrows). Boxes are *p*: southern polar surface, *s*: subantarctic surface, *l*: low-latitude surface, *n*: northern high-latitude surface, *m* thermocline and intermediate, *ds*: deep southern, *dl*: deep low-latitude, *dn*: deep northern box. Model results with isotope fractionation during utilization (represented by the isotope effect ε) prescribed (b) throughout the surface ocean and (c) everywhere in the surface ocean *except* the surface Southern Ocean boxes (filled). It can be seen that the North Atlantic–Southern Ocean δ^{30}Si gradient produced by the control model in Figure 6b disappears in the test case in Figure 6c. Modeled Si concentrations are identical for both model runs.

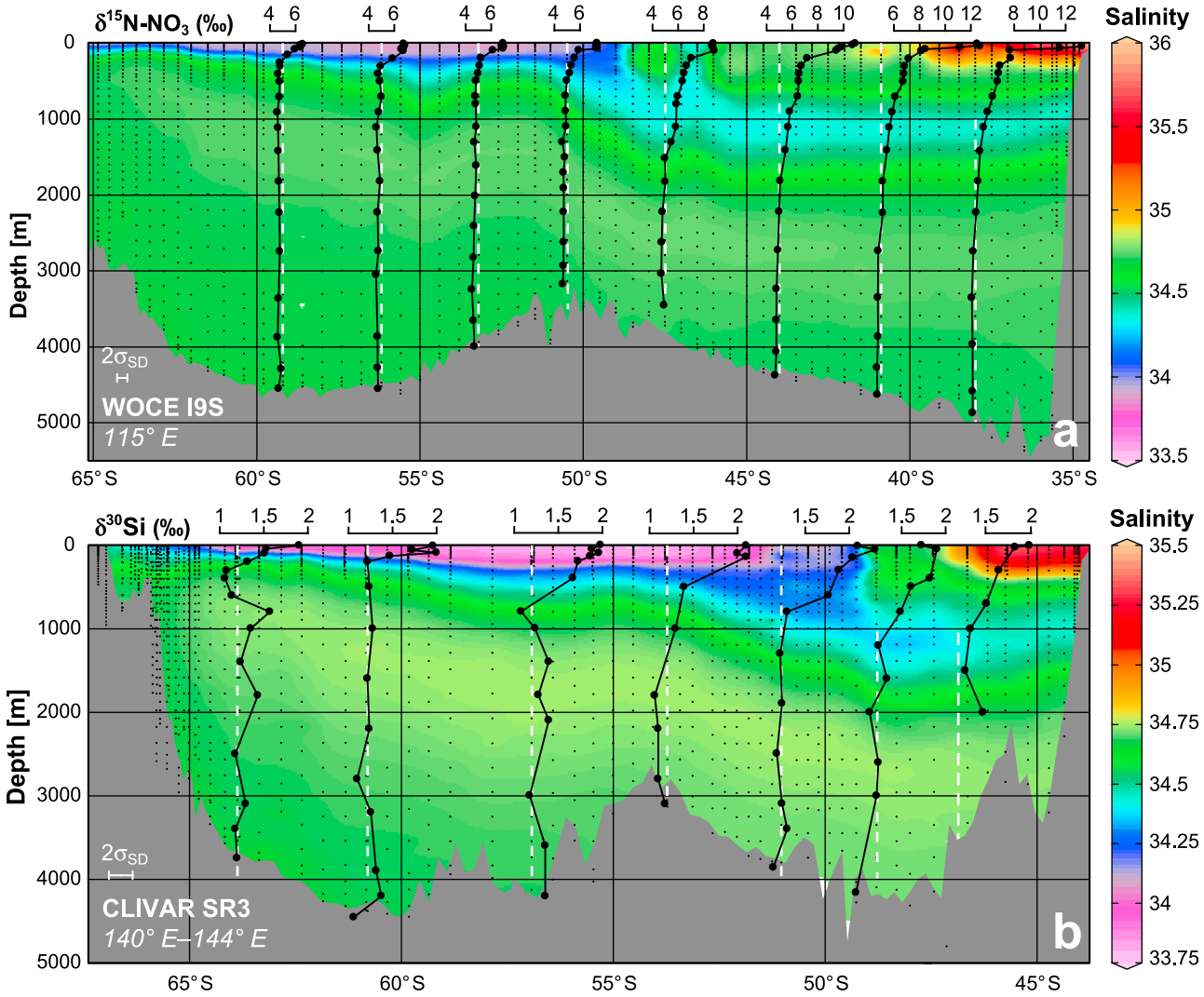

Figure 7. Relationship between water masses and nutrient isotope composition in the Southern Ocean south of Australia. The salinity color map indicates the presence of AAIW in the subsurface as a salinity minimum north of ~50°S. Superimposed on this are depth profiles of (a) δ^{15}N-NO_3 values [*Sigman et al.*, 2000] and (b) δ^{30}Si values [*Cardinal et al.*, 2005]. The δ^{30}Si data show a clear relationship of elevated values in the Subantarctic subsurface associated with the salinity minimum, while δ^{15}N-NO_3 values remain relatively low throughout the Subantarctic subsurface, with large isotopic gradients remaining restricted to the uppermost water column as in the Antarctic [see also *DiFiore et al.*, 2006]. The dashed line in each depth profile marks the sampling position and indicates the isotope composition of the mean deep ocean (Figure 7a, δ^{15}N-NO_3 = +5‰) or the deep Southern Ocean (Figure 7b, δ^{30}Si = +1.2‰). Silicon isotope data are converted from δ^{29}Si using the conversion factor of 1.96 [*Reynolds et al.*, 2006b]. Salinity color maps were created with ODV (R. Schlitzer, Ocean Data View, 2009, available at http://odv.awi.de) using data from the eWOCE [*Schlitzer*, 2000] and CCHDO (http://cchdo.ucsd.edu/) databases.

[26] Figure 7 shows δ^{30}Si and δ^{15}N–NO_3 data from two Southern Ocean transects south of Australia [*Sigman et al.*, 2000; *Cardinal et al.*, 2005]. The δ^{30}Si depth profiles in Figure 7b highlight the fact that elevated δ^{30}Si values in the Subantarctic subsurface are associated with the salinity minimum of AAIW and shallower Subantarctic thermocline waters. Such a relationship is not observed to the same extent for δ^{15}N–NO_3 (Figure 7a), for which the isotopic signature of AAIW is not strongly different from that of the deep Southern Ocean. These observations clearly show that the process of AAIW formation influences its δ^{30}Si and δ^{15}N–NO_3 signatures differently. Below, we explore the likely reasons for this contrasting behavior.

[27] Mass balance calculations by *Fripiat et al.* [2011] indicate that the dominant contributor (97%) to the Si inventory of AAIW is Antarctic Surface Water (AASW) from the Polar Front (PF). Antarctic Surface Water is present from the PF southwards, and bears the properties of the Antarctic winter mixed layer [e.g., *Rintoul and Bullister*, 1999]. Within AASW, Si concentrations decrease strongly

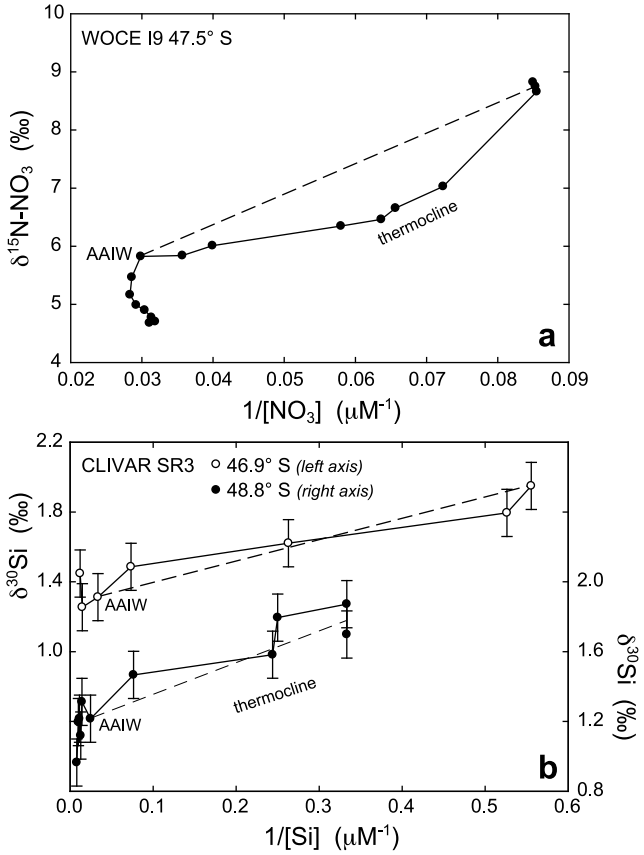

Figure 8. Data from station depth profiles (bottom to surface) plotted in mixing space to illustrate relationships between (a) δ^{15}N-NO$_3$ [*Sigman et al.*, 2000] and (b) δ^{30}Si values [*Cardinal et al.*, 2005] of water masses in the Subantarctic Southern Ocean (error bars are $2\sigma_{SD}$). While δ^{15}N-NO$_3$ values in the Subantarctic thermocline are too low to be explained by mixing in the local water column (dashed line in Figure 8a), δ^{30}Si values are consistent with such a mixing origin (dashed lines in Figure 8b). Silicon isotope data are converted from δ^{29}Si as in Figure 7; the sample denoted AAIW is that closest to the subsurface salinity minimum. Nitrate concentrations were converted to μM using a constant σ_θ of 27 as in *Sigman et al.* [2000].

($\sim$30 μM) northward (i.e. toward the PF), while NO$_3$ concentrations display only a modest decrease ($\sim$3 μM [e.g., *Garcia et al.*, 2010]). This markedly different behavior is likely due to a combination of the high silicification of Southern Ocean diatoms [e.g., *Takeda*, 1998] and the more efficient recycling of NO$_3$ than Si in the surface and shallow subsurface [*Dugdale et al.*, 1995; *Brzezinski et al.*, 2003]. Importantly, the [Si] decrease in AASW toward the north is accompanied by increasing δ^{30}Si values, while δ^{15}N–NO$_3$ values remain essentially constant [*Sigman et al.*, 2000; *Fripiat et al.*, 2011]. Thus at the Polar Front, AASW possesses an elevated δ^{30}Si value of around +1.8‰ [*Fripiat et al.*, 2011], but a δ^{15}N–NO$_3$ value that is virtually indistinguishable from that of the deep Southern Ocean (+5.6‰ [*Sigman et al.*, 2000]). These isotope signatures are imparted to AAIW with virtually no alteration [*Sigman et al.*, 2000; *Fripiat et al.*, 2011]. Thus, the strong utilization of Si by diatoms south of the PF results in an elevated δ^{30}Si signature in AASW that is incorporated into AAIW, while the modest drawdown of NO$_3$ leads to a AAIW δ^{15}N–NO$_3$ signature that is very similar to that of the deep Southern Ocean.

[28] At levels shallower than AAIW, the δ^{15}N–NO$_3$ distribution in the Subantarctic subsurface may be further affected by complexities of the δ^{15}N–NO$_3$ system. *Sigman et al.* [2000] found that δ^{15}N-NO$_3$ values in the Subantarctic thermocline were too low to be explained by mixing in the Subantarctic alone (Figure 8a). They suggested that this feature might be due to the influence of subtropical waters whose isotopic composition has been affected either by nitrogen fixation or by mixing with very N-depleted low-latitude surface waters. The same mixing calculation for the δ^{30}Si data of *Cardinal et al.* [2005] reveals that, unlike δ^{15}N-NO$_3$, δ^{30}Si values in the Subantarctic thermocline are consistent with mixing between Antarctic and Subantarctic waters (Figure 8b), as also concluded by *Fripiat et al.* [2011]. Since mixing with low-nutrient subtropical surface waters should affect both δ^{30}Si and δ^{15}N-NO$_3$ values in the Subantarctic thermocline to a similar degree, the discrepancy between the systematics of these two systems (Figure 8) suggests that the low δ^{15}N-NO$_3$ values in the Subantarctic thermocline result rather from the influence of low-latitude nitrogen fixation.

[29] The arguments above suggest a cause for the difference between the oceanic δ^{30}Si and δ^{15}N-NO$_3$ distribution at the basin scale. First, the different degrees to which Si and NO$_3$ are drawn down by biological production in the Antarctic Zone of the Southern Ocean, likely driven by the more efficient remineralization of NO$_3$ in the shallow subsurface, results in the formation of AAIW that is markedly different in δ^{30}Si, but not in δ^{15}N–NO$_3$, from the deep Southern Ocean. Additionally, δ^{15}N–NO$_3$ values in the Subantarctic thermocline appear to be depressed even at high latitudes due to the influence of regions of nitrogen fixation, a signal that is likely reinforced by "downstream" nitrogen fixation at low northern latitudes [*Knapp et al.*, 2008] that further reduces the δ^{15}N-NO$_3$ of the Atlantic thermocline. No such complexity influences the Si isotope system, such that southern mode and intermediate waters not only (a) form with a higher δ^{30}Si value than the deep Southern Ocean but also (b) can impart this high value to the entire Atlantic thermocline. The MOC-driven nutrient transport into the North Atlantic – the northern loop of Figure 5 – is thus significantly different in δ^{30}Si, but not in δ^{15}N-NO$_3$, from the deep Southern Ocean. The δ^{30}Si and δ^{15}N-NO$_3$ signatures of NADW thus ultimately reflect processes related to the interaction of biology and the physical circulation in the Southern Ocean (nutrient utilization, remineralization, water mass subduction) and the global low-latitude upper ocean (nitrogen fixation, thermocline ventilation, MOC closure).

5. Global δ^{30}Si Distribution: Perspectives

[30] Although the focus of this paper is the biogeochemistry of Si in the Atlantic Ocean, it would be amiss not to briefly discuss this first comprehensive Atlantic δ^{30}Si dataset in the global context. In their "first look" at seawater δ^{30}Si values, *De La Rocha et al.* [2000] argued for a diatom dissolution flux into deepwaters with, on average, a lower δ^{30}Si value than seawater. *Beucher et al.* [2008], in

contrast, utilized a compilation of Southern Ocean and Pacific data to argue for a δ^{30}Si value of the dissolution flux that is higher than that of deepwaters. This study has highlighted the important role, also recognized by *De La Rocha et al.* [2000], that physical processes – i.e. deepwater formation and nutrient transport by the ocean circulation – play in setting deep ocean δ^{30}Si values. We would thus argue that global deepwater δ^{30}Si gradients cannot be interpreted quite as simply as either of these previous contributions has done. Rather, interpretation of the oceanic δ^{30}Si distribution must consider the influence of both biological cycling and ocean circulation – that is, the *remineralized* and *preformed* contributions to the observed δ^{30}Si distribution.

[31] Such analyses may be performed in the quantitative framework of global circulation models (GCMs), provided that these models conform to the observational constraint of a strong deepwater δ^{30}Si gradient, which is not the case for the only published GCM study [*Wischmeyer et al.*, 2003]. *Reynolds* [2009] did reproduce this gradient with box models, but could not adequately explain the disagreement with GCM results. In fact, several plausible reasons exist for the inability of *Wischmeyer et al.*'s [2003] model to produce a deepwater δ^{30}Si gradient. *Dutay et al.* [2002] have demonstrated that the physical model employed by *Wischmeyer et al.* [2003] strongly underestimates the ventilation of intermediate waters, which our analysis would indicate are vital for the production of a large-scale deepwater δ^{30}Si gradient. The poor intermediate water ventilation in *Wischmeyer et al.*'s [2003] model may be due to its representation of lateral mixing [*Maier-Reimer et al.*, 1993], which does not parameterize the advective effects of mesoscale eddies [*Gent and McWilliams*, 1990]. This eddy-induced transport plays an important role in the subduction of water masses in the Southern Ocean [*Marshall*, 1997], and its correct parameterization has been shown to improve GCM representation of the oceanic Si cycle [*Gnanadesikan*, 1999a; *Gnanadesikan and Toggweiler*, 1999; *Dunne et al.*, 2007]. The coupled biological-physical model of *Wischmeyer et al.* [2003] displays its strongest deviation from observational [Si] data in the surface Southern Ocean, suggesting that Si cycling in this region is inaccurately captured. Furthermore, their physical model employed an upwind tracer advection scheme [*Maier-Reimer et al.*, 1993] that results in large numerical diffusion [e.g., *Gerya*, 2010]. This implicit strong mixing may inhibit large isotopic gradients at depth, as well as diluting any high-δ^{30}Si signal in intermediate waters by strong vertical mixing with the deep. The combination of these dynamical and biogeochemical weaknesses may have prevented *Wischmeyer et al.*'s [2003] model from forming southern intermediate and mode waters with the correct biogeochemical properties, such that it did not accurately represent the northward MOC-driven nutrient transport. Future modeling efforts should focus on reproducing the large-scale, first-order observational constraints that we have documented here.

6. Summary and Conclusions

[32] Our high-precision δ^{30}Si dataset for the Atlantic Ocean demonstrates the strength of seawater δ^{30}Si as a tracer of the biogeochemical cycling of Si in the sea. The stable isotope composition of dissolved silicon traces mixing between water masses of North Atlantic and Southern Ocean origin, which implies that Si has no significant sources or sinks at depth in the Atlantic Ocean. The contrasting δ^{30}Si values of the North Atlantic and the deep Southern Ocean are, in turn, most likely the result of the fractionation signature introduced into the thermocline by the interaction of biological Si uptake with mode- and intermediate-water mass formation at high southern latitudes. Biological activity in the surface Southern Ocean thus imparts distinct δ^{30}Si values to the two "loops" of *Toggweiler et al.*'s [2006] MOC representation, with the large-scale interaction of these loops producing the basin-scale Atlantic δ^{30}Si distribution.

[33] The Si isotope data presented here thus provide strong evidence for a regime of nutrient transport in the ocean that is closely coupled to lateral transports related to the MOC. In combination with our box-modeling approach, the δ^{30}Si data robustly and independently corroborate previous inferences [*Sarmiento et al.*, 2004] of the importance of the Southern Ocean's biogeochemical divide [*Marinov et al.*, 2006] in determining global oceanic nutrient distributions, and thus the distribution and magnitude of oceanic primary productivity. Furthermore, the pathways of large-scale tracer transport in the ocean are directly relevant to the fundamental mechanisms driving the MOC [*Gnanadesikan*, 1999b]. The insights provided by seawater δ^{30}Si data thus reach far beyond the oceanic Si cycle and touch upon fundamental questions in modern oceanography.

[34] **Acknowledgments.** The authors would like to thank the captain and crew of R/Vs *Polarstern*, *Knorr* and *Pelagia* as well as M. Rutgers van der Loeff as Chief Scientist on cruise ANT XXIII/1. P. Laan and J. de Jong are gratefully acknowledged for sampling on cruise 64PE319. Feedback from Nicolas Gruber helped to considerably improve an earlier version of this manuscript. Two anonymous reviewers are thanked for their constructive input. This work was supported by Swiss National Science Foundation grants 200021-116473 and 200020-130361.

References

Albarède, F. (1996), *Introduction to Geochemical Modeling*, Cambridge Univ. Press, Cambridge, U. K.

Anderson, L. A., and J. L. Sarmiento (1994), Redfield ratios of remineralization determined by nutrient data analysis, *Global Biogeochem. Cycles*, *8*, 65–80.

Beucher, C. P., M. A. Brzezinski, and J. L. Jones (2008), Sources and biological fractionation of silicon isotopes in the eastern equatorial Pacific, *Geochim. Cosmochim. Acta*, *72*, 3063–3073.

Brambilla, E., L. D. Talley, and P. E. Robbins (2008), Subpolar Mode Water in the northeastern Atlantic: 2. Origin and transformation, *J. Geophys. Res.*, *113*, C04026, doi:10.1029/2006JC004063.

Broecker, W. S., T. Takahashi, and Y.-H. Li (1976), Hydrography of the central Atlantic—I. The two-degree discontinuity, *Deep Sea Res.*, *23*, 1083–1104.

Broecker, W. S., S. Blanton, W. M. Smethie, and G. Ostlund (1991), Radiocarbon decay and oxygen utilization in the deep Atlantic Ocean, *Global Biogeochem. Cycles*, *5*, 87–117.

Brzezinski, M. A., C. J. Pride, V. M. Franck, D. M. Sigman, J. L. Sarmiento, K. Matsumoto, N. Gruber, G. H. Rau, and K. H. Coale (2002), A switch from $Si(OH)_4$ to NO_3^- depletion in the glacial Southern Ocean, *Geophys. Res. Lett.*, *29*(12), 1564, doi:10.1029/2001GL014349.

Brzezinski, M. A., M. L. Dickson, D. M. Nelson, and R. Sambrotto (2003), Ratios of Si, C and N uptake by microplankton in the Southern Ocean, *Deep Sea Res., Part II*, *50*, 619–633.

Brzezinski, M. A., J. L. Jones, C. P. Beucher, M. S. Demarest, and H. L. Berg (2006), Automated determination of silicon isotope natural abundance by the acid decomposition of cesium hexafluosilicate, *Anal. Chem.*, *78*, 6109–6114.

Cardinal, D., L. Y. Alleman, F. Dehairs, N. Savoye, T. W. Trull, and L. André (2005), Relevance of silicon isotopes to Si-nutrient utilization and Si-source assessment in Antarctic waters, *Global Biogeochem. Cycles*, *19*, GB2007, doi:10.1029/2004GB002364.

Chisholm, S. W., and F. M. M. Morel (1991), Special issue: What controls phytoplankton production in nutrient-rich areas of the open sea?, *Limnol. Oceanogr.*, *36*, 1507–1970.

Crosta, X., C. Beucher, K. Pahnke, and M. A. Brzezinski (2007), Silicic acid leakage from the Southern Ocean: Opposing effects of nutrient uptake and oceanic circulation, *Geophys. Res. Lett.*, *34*, L13601, doi:10.1029/2006GL029083.

De La Rocha, C. L., M. A. Brzezinski, and M. J. DeNiro (1997), Fractionation of silicon isotopes by marine diatoms during biogenic silica formation, *Geochim. Cosmochim. Acta*, *61*, 5051–5056.

De La Rocha, C. L., M. A. Brzezinski, M. J. DeNiro, and A. Shemesh (1998), Silicon-isotope composition of diatoms as an indicator of past oceanic change, *Nature*, *395*, 680–683.

De La Rocha, C. L., M. A. Brzezinski, and M. J. DeNiro (2000), A first look at the distribution of the stable isotopes of silicon in natural waters, *Geochim. Cosmochim. Acta*, *64*, 2467–2477.

Dickson, R. R., and J. Brown (1994), The production of North Atlantic Deep Water: Sources, rates, and pathways, *J. Geophys. Res.*, *99*, 12,319–12,341.

DiFiore, P. J., D. M. Sigman, T. W. Trull, M. J. Lourey, K. Karsh, G. Cane, and R. Ho (2006), Nitrogen isotope constraints on subantarctic biogeochemistry, *J. Geophys. Res.*, *111*, C08016, doi:10.1029/2005JC003216.

Dugdale, R. C., F. P. Wilkerson, and H. J. Minas (1995), The role of a silicate pump in driving new production, *Deep Sea Res., Part I*, *42*, 697–719.

Dunne, J. P., J. L. Sarmiento, and A. Gnanadesikan (2007), A synthesis of global particle export from the surface ocean and cycling through the ocean interior and on the seafloor, *Global Biogeochem. Cycles*, *21*, GB4006, doi:10.1029/2006GB002907.

Dutay, J. C., et al. (2002), Evaluation of ocean model ventilation with CFC-11: Comparison of 13 global ocean models, *Ocean Modell.*, *4*, 89–120.

Eldevik, T., J. E. O. Nilsen, D. Iovino, K. Anders Olsson, A. B. Sando, and H. Drange (2009), Observed sources and variability of Nordic seas overflow, *Nat. Geosci.*, *2*, 406–410.

Foster, T. D., and E. C. Carmack (1976), Frontal zone mixing and Antarctic Bottom Water formation in the southern Weddell Sea, *Deep Sea Res. Oceanogr. Abstr.*, *23*, 301–317.

Fripiat, F., A.-J. Cavagna, F. Dehairs, S. Speich, L. André, and D. Cardinal (2011), Silicon pool dynamics and biogenic silica export in the Southern Ocean, inferred from Si-isotopes, *Ocean Sci.*, *7*, 533–547.

Ganachaud, A., and C. Wunsch (2000), Improved estimates of global ocean circulation, heat transport and mixing from hydrographic data, *Nature*, *408*, 453–457.

Garcia, H. E., R. A. Locarnini, T. P. Boyer, and J. I. Antonov (2010), *World Ocean Atlas 2009*, vol. 4, *Nutrients (Phosphate, Nitrate, Silicate)*, *NOAA Atlas NESDIS*, vol. 71, U.S. Gov. Print. Off., Washington, D. C.

Gent, P. R., and J. C. McWilliams (1990), Isopycnal mixing in ocean circulation models, *J. Phys. Oceanogr.*, *20*, 150–155.

Georg, R., B. Reynolds, M. Frank, and A. Halliday (2006), New sample preparation techniques for the determination of Si isotopic compositions using MC-ICPMS, *Chem. Geol.*, *235*, 95–104.

Gerya, T. (2010), *Introduction to Numerical Geodynamic Modelling*, Cambridge Univ. Press, Cambridge, U. K.

Gnanadesikan, A. (1999a), A global model of silicon cycling: Sensitivity to eddy parametrization and dissolution, *Global Biogeochem. Cycles*, *13*, 199–220.

Gnanadesikan, A. (1999b), A simple predictive model for the structure of the oceanic pycnocline, *Science*, *283*, 2077–2079.

Gnanadesikan, A., and J. R. Toggweiler (1999), Constraints placed by silicon cycling on vertical exchange in general circulation models, *Geophys. Res. Lett.*, *26*, 1865–1868.

Gruber, N. (1998), Anthropogenic CO_2 in the Atlantic Ocean, *Global Biogeochem. Cycles*, *12*, 165–191.

Gruber, N., et al. (2009), Oceanic sources, sinks, and transport of atmospheric CO_2, *Global Biogeochem. Cycles*, *23*, GB1005, doi:10.1029/2008GB003349.

Hansen, B., and S. Østerhus (2000), North Atlantic–Nordic Seas exchanges, *Prog. Oceanogr.*, *45*, 109–208.

Holfort, J., and G. Siedler (2001), The meridional oceanic transports of heat and nutrients in the South Atlantic, *J. Phys. Oceanogr.*, *31*, 5–29.

Huhn, O., H. H. Hellmer, M. Rhein, C. Rodehacke, W. Roether, M. P. Schodlok, and M. Schröder (2008), Evidence of deep- and bottom-water formation in the western Weddell Sea, *Deep Sea Res., Part II*, *55*, 1098–1116.

Jeandel, C., Y. Godderis, B. Peucker-Ehrenbrink, F. Lacan, and T. Arsouze (2009), Impact of the boundary processes on Si, Ca and Mg inputs to the ocean, *Geochim. Cosmochim. Acta*, *73*, A588.

Jin, X., N. Gruber, J. P. Dunne, J. L. Sarmiento, and R. A. Armstrong (2006), Diagnosing the contribution of phytoplankton functional groups to the production and export of particulate organic carbon, $CaCO_3$, and opal from global nutrient and alkalinity distributions, *Global Biogeochem. Cycles*, *20*, GB2015, doi:10.1029/2005GB002532.

Karl, D. M., and G. Tien (1992), MAGIC: A sensitive and precise method for measuring dissolved phosphorus in aquatic environments, *Limnol. Oceanogr.*, *37*, 105–116.

Kawase, M., and J. L. Sarmiento (1985), Nutrients in the Atlantic thermocline, *J. Geophys. Res.*, *90*, 8961–8979.

Knapp, A. N., P. J. DiFiore, C. Deutsch, D. M. Sigman, and F. Lipschultz (2008), Nitrate isotopic composition between Bermuda and Puerto Rico: Implications for N_2 fixation in the Atlantic Ocean, *Global Biogeochem. Cycles*, *22*, GB3014, doi:10.1029/2007GB003107.

Larqué, L., K. Maamaatuaiahutapu, and V. Garçon (1997), On the intermediate and deep water flows in the South Atlantic Ocean, *J. Geophys. Res.*, *102*, 12,425–12,440.

Ledwell, J. R., A. J. Watson, and C. S. Law (1993), Evidence for slow mixing across the pycnocline from an open-ocean tracer-release experiment, *Nature*, *364*, 701–703, doi:10.1038/364701a0.

Lumpkin, R., and K. Speer (2003), Large-scale vertical and horizontal circulation in the North Atlantic Ocean, *J. Phys. Oceanogr.*, *33*, 1902–1920.

Lumpkin, R., and K. Speer (2007), Global ocean meridional overturning, *J. Phys. Oceanogr.*, *37*, 2550–2562.

Maier-Reimer, E., U. Mikolajewicz, and K. Hasselmann (1993), Mean circulation of the Hamburg LSG OGCM and its sensitivity to the thermohaline surface forcing, *J. Phys. Oceanogr.*, *23*, 731–757.

Mantyla, A. W., and J. L. Reid (1983), Abyssal characteristics of the world ocean waters, *Deep Sea Res., Part A*, *30*, 805–833.

Margalef, R. (1978), Life-forms of phytoplankton as survival alternatives in an unstable environment, *Oceanol. Acta*, *1*, 493–509.

Marinov, I., A. Gnanadesikan, J. R. Toggweiler, and J. L. Sarmiento (2006), The Southern Ocean biogeochemical divide, *Nature*, *441*, 964–967.

Marshall, D. (1997), Subduction of water masses in an eddying ocean, *J. Mar. Res.*, *55*, 201–222.

Matsumoto, K. (2007), Radiocarbon-based circulation age of the world oceans, *J. Geophys. Res.*, *112*, C09004, doi:10.1029/2007JC004095.

Matsumoto, K., J. L. Sarmiento, and M. A. Brzezinski (2002), Silicic acid leakage from the Southern Ocean: A possible explanation for glacial atmospheric pCO_2, *Global Biogeochem. Cycles*, *16*(3), 1031, doi:10.1029/2001GB001442.

Mauritzen, C. (1996), Production of dense overflow waters feeding the North Atlantic across the Greenland-Scotland Ridge. Part 1: Evidence for a revised circulation scheme, *Deep Sea Res., Part I*, *43*, 769–806.

McCartney, M. S., and C. Mauritzen (2001), On the origin of the warm inflow to the Nordic Seas, *Prog. Oceanogr.*, *51*, 125–214.

McCartney, M. S., and L. D. Talley (1982), The Subpolar Mode Water of the North Atlantic Ocean, *J. Phys. Oceanogr.*, *12*, 1169–1188.

Orsi, A. H., G. C. Johnson, and J. L. Bullister (1999), Circulation, mixing, and production of Antarctic Bottom Water, *Prog. Oceanogr.*, *43*, 55–109.

Palter, J. B., and M. S. Lozier (2008), On the source of Gulf Stream nutrients, *J. Geophys. Res.*, *113*, C06018, doi:10.1029/2007JC004611.

Palter, J. B., J. L. Sarmiento, A. Gnanadesikan, J. Simeon, and R. D. Slater (2010), Fueling export production: Nutrient return pathways from the deep ocean and their dependence on the meridional overturning circulation, *Biogeosciences*, *7*, 3549–3568.

Pichevin, L., B. C. Reynolds, R. S. Ganeshram, I. Cacho, L. Pena, K. Keefe, and R. M. Ellam (2009), Enhanced carbon pump inferred from relaxation of nutrient limitation in the glacial ocean, *Nature*, *459*, 1114–1117.

Ragueneau, O., et al. (2000), A review of the Si cycle in the modern ocean: Recent progress and missing gaps in the application of biogenic opal as a paleoproductivity proxy, *Global Planet. Change*, *26*, 317–365.

Ragueneau, O., A. Regaudie-de Gioux, B. Moriceau, M. Gallinari, A. Vangriesheim, F. Baurand, and A. Khripounoff (2009), A benthic Si mass balance on the Congo margin: Origin of the 4000 m DSi anomaly and implications for the transfer of Si from land to ocean, *Deep Sea Res., Part II*, *56*, 2197–2207.

Reid, J. L. (1989), On the total geostrophic circulation of the South Atlantic Ocean: Flow patterns, tracers, and transports, *Prog. Oceanogr.*, *23*, 149–244.

Reynolds, B. C. (2009), Modeling the modern marine δ^{30}Si distribution, *Global Biogeochem. Cycles*, *23*, GB2015, doi:10.1029/2008GB003266.

Reynolds, B. C., M. Frank, and A. N. Halliday (2006a), Silicon isotope fractionation during nutrient utilization in the North Pacific, *Earth Planet. Sci. Lett.*, *244*, 431–443.

Reynolds, B. C., R. B. Georg, F. Oberli, U. Wiechert, and A. N. Halliday (2006b), Re-assessment of silicon isotope reference materials using high-resolution multi-collector ICP-MS, *J. Anal. At. Spectr.*, *21*, 266–269.

Reynolds, B. C., et al. (2007), An inter-laboratory comparison of Si isotope reference materials, *J. Anal. At. Spectr.*, *22*, 561–568.

Rickli, J., M. Frank, and A. N. Halliday (2009), The hafnium-neodymium isotopic composition of Atlantic seawater, *Earth Planet. Sci. Lett.*, *280*, 118–127.

Rintoul, S. R., and J. L. Bullister (1999), A late winter hydrographic section from Tasmania to Antarctica, *Deep Sea Res., Part I*, *46*, 1417–1454.

Rintoul, S. R., and C. Wunsch (1991), Mass, heat, oxygen and nutrient fluxes and budgets in the North Atlantic Ocean, *Deep Sea Res.*, *38*, suppl. 1, S355–S377.

Sallée, J.-B., K. Speer, S. Rintoul, and S. Wijffels (2010), Southern Ocean thermocline ventilation, *J. Phys. Oceanogr.*, *40*, 509–529.

Sarmiento, J. L., N. Gruber, M. A. Brzezinski, and J. P. Dunne (2004), High-latitude controls of thermocline nutrients and low latitude biological productivity, *Nature*, *427*, 56–60.

Sarmiento, J. L., J. Simeon, A. Gnanadesikan, N. Gruber, R. M. Key, and R. Schlitzer (2007), Deep ocean biogeochemistry of silicic acid and nitrate, *Global Biogeochem. Cycles*, *21*, GB1S90, doi:10.1029/2006GB002720.

Schlitzer, R. (2000), Electronic atlas of WOCE hydrographic and tracer data now available, *Eos Trans. AGU*, *81*, 45.

Schmittner, A., N. M. Urban, K. Keller, and D. Matthews (2009), Using tracer observations to reduce the uncertainty of ocean diapycnal mixing and climate–carbon cycle projections, *Global Biogeochem. Cycles*, *23*, GB4009, doi:10.1029/2008GB003421.

Schmitz, W. J. (1995), On the interbasin-scale thermohaline circulation, *Rev. Geophys.*, *33*, 151–173.

Schmitz, W. J. (1996), Some global features/North Atlantic Circulation, technical report, Woods Hole Oceanogr. Inst., Woods Hole, Mass.

Schmitz, W. J., and M. S. McCartney (1993), On the North Atlantic circulation, *Rev. Geophys.*, *31*, 29–49.

Sigman, D. M., M. A. Altabet, D. C. McCorkle, R. Francois, and G. Fischer (2000), The δ^{15}N of nitrate in the Southern Ocean: Nitrogen cycling and circulation in the ocean interior, *J. Geophys. Res.*, *105*, 19,599–19,614.

Sigman, D. M., P. J. DiFiore, M. P. Hain, C. Deutsch, Y. Wang, D. M. Karl, A. N. Knapp, M. F. Lehmann, and S. Pantoja (2009), The dual isotopes of deep nitrogen as a constraint on the cycle and budget of oceanic fixed nitrogen, *Deep Sea Res., Part I*, *56*, 1419–1439.

Sloyan, B. M., and S. R. Rintoul (2001), The Southern Ocean limb of the global deep overturning circulation, *J. Phys. Oceanogr.*, *31*, 143–173.

Smetacek, V. (1999), Diatoms and the ocean carbon cycle, *Protist*, *150*, 25–32.

Stramma, L., and M. England (1999), On the water masses and mean circulation of the South Atlantic Ocean, *J. Geophys. Res.*, *104*, 20,863–20,883.

Strickland, J., and T. Parsons (1968), *A Practical Handbook of Seawater Analysis*, *Bull. Fish. Res. Board Can.*, *167*.

Takeda, S. (1998), Influence of iron availability on nutrient consumption ratio of diatoms in oceanic waters, *Nature*, *393*, 774–777.

Tipper, E. T., P. Louvat, F. Capmas, A. Galy, and J. Gaillardet (2008), Accuracy of stable Mg and Ca isotope data obtained by MC-ICP-MS using the standard addition method, *Chem. Geol.*, *257*, 65–75.

Toggweiler, J. R. (1999), Variation of atmospheric CO_2 by ventilation of the ocean's deepest water, *Paleoceanography*, *14*, 571–588.

Toggweiler, J. R., and B. Samuels (1993), New radiocarbon constraints on the upwelling of abyssal water to the ocean's surface, in *The Global Carbon Cycle*, *NATO ASI Ser., Ser. I, Global Environ. Change*, vol. 15, edited by M. Heimann, pp. 333–366, Springer, Berlin.

Toggweiler, J. R., J. L. Russell, and S. R. Carson (2006), Midlatitude westerlies, atmospheric CO_2, and climate change during the ice ages, *Paleoceanography*, *21*, PA2005, doi:10.1029/2005PA001154.

Toole, J. M., K. L. Polzin, and R. W. Schmitt (1994), Estimates of diapycnal mixing in the abyssal ocean, *Science*, *264*, 1120–1123.

Tréguer, P., D. M. Nelson, A. J. van Bennekom, D. J. Demaster, A. Leynaert, and B. Queguiner (1995), The silica balance in the world ocean—A reestimate, *Science*, *268*, 375–379.

Tsuchiya, M. (1989), Circulation of the Antarctic Intermediate Water in the North Atlantic Ocean, *J. Mar. Res.*, *47*, 747–755.

Tsuchiya, M., L. D. Talley, and M. S. McCartney (1994), Water-mass distributions in the western South Atlantic: A section from South Georgia Island (54°S) northward across the equator, *J. Mar. Res.*, *52*, 55–81.

van Bennekom, A. J., and G. W. Berger (1984), Hydrography and silica budget of the Angola Basin, *Neth. J. Sea Res.*, *17*, 149–200.

van den Boorn, S. H. J. M., P. Z. Vroon, and M. J. van Bergen (2009), Sulfur-induced offsets in MC-ICP-MS silicon-isotope measurements, *J. Anal. At. Spectr.*, *24*, 1111–1114.

Varela, D. E., C. J. Pride, and M. A. Brzezinski (2004), Biological fractionation of silicon isotopes in Southern Ocean surface waters, *Global Biogeochem. Cycles*, *18*, GB1047, doi:10.1029/2003GB002140.

Warren, B. (1981), Deep circulation of the world ocean, in *Evolution of Physical Oceanography*, edited by B. Warren and C. Wunsch, pp. 6–41, MIT Press, Cambridge, Mass.

Williams, R. G., V. Roussenov, and M. J. Follows (2006), Nutrient streams and their induction into the mixed layer, *Global Biogeochem. Cycles*, *20*, GB1016, doi:10.1029/2005GB002586.

Wischmeyer, A. G., C. L. De La Rocha, E. Maier-Reimer, and D. A. Wolf-Gladrow (2003), Control mechanisms for the oceanic distribution of silicon isotopes, *Global Biogeochem. Cycles*, *17*(3), 1083, doi:10.1029/2002GB002022.

Wüst, G. (1935), *Wissenschaftliche Ergebnisse der Deutschen Atlantischen Expedition 'Meteor' 1925–1927*, vol. 6, *Schichtung und Zirkulation des Atlantischen Ozeans: Die Stratosphäre*, Notgem. der Dtsch. Wiss., Berlin.